

Cite this article as: Fang Wenqian, Shen Jianran, Yan Jikang, et al. Effect of Er Content on Microstructure and Mechanical Properties of ZL201A Aluminum Alloy[J]. Rare Metal Materials and Engineering, 2023, 52(07): 2326-2334.

ARTICLE

Effect of Er Content on Microstructure and Mechanical Properties of ZL201A Aluminum Alloy

Fang Wenqian¹, Shen Jianran¹, Yan Jikang^{1,2}, Leng Chongyan¹, Gan Guoyou¹

¹ Faculty of Materials Science and Engineering, Kunming University of Science and Technology, Kunming 650093, China; ² School of Engineering, Southwest Petroleum University, Nanchong 637001, China

Abstract: The effects of Er addition on the microstructure and mechanical properties of ZL201A aluminum alloy were studied via metallographic microscope, scanning electron microscope, transmission electron microscope, energy dispersive spectrometer, and mechanical property tests. Results show that the Er addition can refine the α -Al matrix from columnar grains into fine equiaxed grains. Additionally, the θ phase (Al_2Cu) is transformed from fine network structure into the dispersed fine particle structure. When the Er content reaches 0.4wt%, the grain refinement effect reaches the maximum state and the mechanical properties of the alloy are optimal. The average grain size of α -Al matrix is 19 μm ; the tensile strength and the elongation are 298.14 MPa and 6.56%, respectively. The fracture mode also changes from brittle fracture to ductile-brittle fracture, which is beneficial to the practical application of aluminum alloys. When Er content exceeds 0.4wt%, the grain size increases and the mechanical properties of alloy decrease.

Key words: ZL201A; Er element; grain refinement; θ phase metamorphism; mechanical properties

Lightweight automobile is of great application significance and attracts much attention. As-cast aluminum alloy is beneficial to manufacture the lightweight automotive parts, because the aluminum alloy surface usually has dense oxide film and better corrosion resistance. The density of aluminum alloy is about one third of that of steel, therefore reducing nearly 40% mass under the same mechanical requirements. In addition, the production process of aluminum alloy is simple. As a result, aluminum alloys are ideal for mass reduction with proper mechanical properties^[1-3]. However, Fe, Si, and Mg impurities often exist in ZL201A aluminum alloy^[4-5]. The Fe impurity depletes the Cu and Mn in the solid solution and forms $\text{Al}_7\text{Cu}_2\text{Fe}$, $\text{Al}_{10}\text{Mn}_2\text{Si}$, and AlMnFeSi inclusions, thereby decreasing the strength and plasticity of aluminum alloys^[6-7]. Si impurities accelerate the diffusion of Cu and Mn, reduce the solubility of solid solution, and promote the precipitation of the θ (Al_2Cu) and T ($\text{Al}_{12}\text{CuMn}_2$) phases along the grain boundaries in the material, thus decreasing the strength and plasticity of aluminum alloys^[7]. Mg impurities have a significant influence on the alloy performance during casting pro-

cess. When Mg content exceeds 0.05wt%, the $\alpha+\theta(\text{Al}_2\text{Cu})+\text{S}$ (Al_2CuMg) ternary co-crystal with low melting point (507 °C) is formed, which leads to the easy occurrence of crack under thermal stress and increases the probability of overturning during quenching^[8]. Thus, the improvement mechanism of ZL201A aluminum alloy is usually related to the densification of θ phase, grain size refinement, and the modification of impurities.

Grain refinement in ZL201A alloy typically relies on the addition of rare earth elements, Al-Ti, Al-Ti-B, and Al-Ti-C compounds. Kashyap et al^[9] reported that after the addition of Al-Ti intermediate alloy into aluminum melt, Ti reacts with Al, forming Al_3Ti compound. Sigworth^[10] found that the addition of Al-Ti-B intermediate alloy results in the generation of Al_3Ti , AlB_2 , and TiB_2 phases, which act as heterogeneous nucleation cores, thereby promoting the nucleation of α -Al and inhibiting the growth of α -Al grains^[11]. However, the Ti element reacts with impurities in the aluminum alloy, reducing or eliminating the refining ability of Ti. The addition of rare earth elements can purify and densify the θ phase in the

Received date: November 10, 2023

Foundation item: Major Science and Technology Project in Yunnan Province-New Material Special Project (2018ZE005, 2019ZE001)

Corresponding author: Yan Jikang, Ph. D., Professor, School of Engineering, Southwest Petroleum University, Nanchong 637001, P. R. China, E-mail: yanjk@swpu.edu.cn

Copyright © 2023, Northwest Institute for Nonferrous Metal Research. Published by Science Press. All rights reserved.

material, and it also has a stable and long-lasting grain-refinement effect^[12-13].

The rare earth element Er can reduce the content of hydrogen, oxygen, and sulfur in aluminum alloys^[14]. Besides, the Er addition can also reduce gas content through reactions in the liquid aluminum alloys, thereby forming insoluble substances. In addition, Er can react with harmful impurities with low melting points to produce binary compounds with high melting points, low densities, and stable chemical properties, which effectively eliminates the impurities in alloys. The residual particles become heterogeneous nuclei of aluminum alloys and thus refine the grain size^[15-16]. The atomic radius of Er is larger than that of Al, and its properties are relatively more active. Melting Er in liquid aluminum can easily fill the surface defects of aluminum alloys, which reduces the surface tension at the interface between the old and new phases and increases the growth rate of nuclei. Furthermore, Er can form a surface-active film between the solid grains and molten liquid, preventing the grain growth and thus refining the grain structure of alloys^[17-18]. The Er addition in Al-Cu system forms a better interfacial relationship, generating the Al_3Er and $\text{Al}_8\text{Cu}_4\text{Er}$ compounds, which promotes the formation of α -Al dendrite structure and improves the performance of aluminum alloys^[19-23]. The effects of the addition of rare earth elements on the structure and properties of aluminum alloys have been extensively researched, but the effects of Er content on the refinement, microstructure evolution, and mechanical properties of the ZL201A alloy are rarely discussed.

In this research, the effect of Er addition on the microstructure and mechanical properties of ZL201A alloy was investigated through microstructure analysis and property evaluation. Besides, the strengthening mechanism was also studied.

1 Experiment

Six groups of alloys with different components were prepared from 99.99Al, 99.99Cu, 99.99Mn, Al-75Ti, and Al-10Er master alloy, and their composition is shown in Table 1. The mass of to-be-melted materials was calculated and weighed as design. Then, the materials were loaded in the graphite crucible and heated to 750 °C in a resistance furnace. After the alloy was completely melted, the melt was drained

Table 1 Composition of ZL201A aluminum alloy with different Er contents (wt%)

Cu	Mn	Ti	Er	Al
			0.0	
			0.1	
			0.2	
5.2	0.8	0.3	0.3	Bal.
			0.4	
			0.45	
			0.5	

and the slag was removed by refining agent. Subsequently, the as-prepared master alloy was pressed into the bottom of liquid aluminum with a bell cover, and once the intermediate alloy was melted, a covering agent was added to prevent the absorption of molten aluminum during the heat preservation process. After heating at 750 °C for 20 min, the alloy elements were homogenized via manual stirring for 5 min. Finally, the furnace temperature reduced to 720 °C, the slag was completely removed, and the liquid metal was poured into the metal mold (preheated to 300 °C), therefore forming the cylindrical aluminum ingots with diameter of 15 or 200 mm.

The specimens were obtained from the middle of the aluminum ingot by cutting machine, and then subjected to rough grinding, fine grinding, polishing, and surface etching (Keller's etching agent, about 15 s). Finally, the specimens were cleaned by alcohol and dried by air. The microstructure and morphologies of specimens were observed by TX-400V optical microscope (OM), JSM-6490LV scanning electron microscope (SEM), and JEM-2100 transmission electron microscope (TEM) with selected area electron diffraction (SAED) analysis. The composition was analyzed by X-ray diffractometer (XRD). The mechanical properties were obtained through WAW-300 universal tensile tester and MVSD-FX automatic microhardness tester.

2 Results and Discussion

2.1 Phase analysis

In order to analyze the effect of solidification on the microstructure and mechanical properties of ZL201A aluminum alloy, the phase diagrams of Al-Er and Al-Cu alloys were calculated under the consideration of their thermodynamics. Fig. 1 shows the phase diagram of Al-Er alloy. When Er content is 0.1wt%–0.5wt%, the liquidus temperature is 740 °C, and partial α -Al phase is precipitated with decreasing the temperature. The solidus temperature is 670 °C, and hexagonal Er and α -Al phases exist at temperatures between the solidus temperature and room temperature. Er was added in front of the solid-liquid boundary during melt solidification, resulting in the composition undercooling. Er of high melting point (1529 °C) can be used as

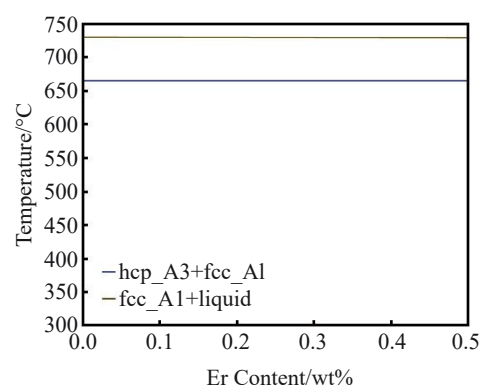


Fig.1 Thermodynamically calculated phase diagram of Al-Er alloy

heterogeneous nucleation in the melt, thus increasing the number of nucleation points, which leads to the grain refinement^[24].

Fig. 2 shows the thermodynamic phase diagram of Al-Cu alloy. Cu is an important element for the formation of θ phase in the alloy. With increasing the Cu content from 0wt% to 6wt%, the melting point of alloy is decreased from 660 °C to 645 °C. With decreasing the temperature, the α -Al phase precipitated in the liquid phase forms a solid-liquid dual phase region. When the Cu content is higher than 5.8wt% and the temperature is lower than 550 °C, the remaining liquid phase undergoes a eutectic reaction to form θ and α -Al phases. When the Cu content is less than 5.8wt%, all the Cu atoms are dissolved into α -Al phase at the melting temperature, and the remaining liquid phase is completely transformed into the α -Al phase. With decreasing the temperature, the solid solubility of Cu atoms is reduced and the θ phase is precipitated from the α -Al phase. In the ZL201A aluminum alloy with 5.2wt% Cu, the alloy can be solidified to form α -Al phase and then dissolved into the θ phase. However, due to the redistribution of solute during the solidification process and the increase in Cu content, the eutectic reaction can also occur in the ZL201A aluminum alloy to form the θ and α -Al phases. Therefore, the θ phase in ZL201A aluminum alloy at room temperature is composed of eutectic and undissolved structures. For the ZL201A aluminum alloy with 5.2wt% Cu, the solidus temperature is 554 °C, and the maximum dissolution temperature is 530 °C. In this temperature range, the solid phase is in the α -Al phase, and the supersaturated solid solution can also be formed by heat treatment to improve the mechanical properties of material^[25-26].

Fig. 3 shows XRD patterns of ZL201A aluminum alloy with different Er contents. Sharp diffraction peaks can be observed at $2\theta=38.2^\circ$, 45.4° , 65.1° , 77.8° , and 82.7° , which are consistent with the characteristic peaks of (111), (200), (220), (311), and (222) crystal faces of face-centered cubic (fcc) aluminum, respectively. XRD diffraction peaks can also be seen at $2\theta=21^\circ$, 42.6° , and 47.8° , corresponding to the characteristic peaks of (110), (112), and (202) crystal faces, respectively, indicating the body-centered cubic (bcc) Al_2Cu . Compared with that of ZL201A aluminum alloy, an extra

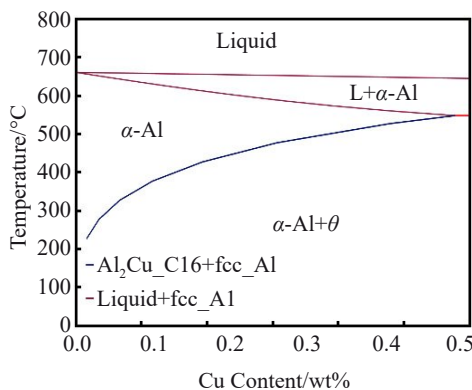


Fig. 2 Thermodynamically calculated phase diagram of Al-Cu alloy

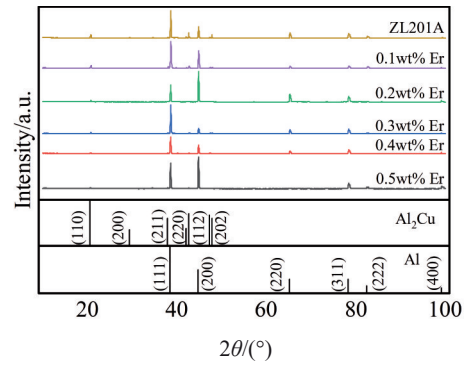


Fig. 3 XRD patterns of ZL201A aluminum alloy with different Er contents

diffraction peak at $2\theta=99^\circ$ appears after Er addition, indicating the fcc aluminum. Besides, the ZL201A alloy with Er addition does not have the diffraction peaks at $2\theta=42.6^\circ$, 47.8° . Additionally, according to the decrease in the intensity of diffraction peak of θ phase and the increase in the intensity of Al diffraction peak, it can be inferred that the Cu atoms are dissolved in the α -Al matrix, and thus the θ phase is decreased. The primary functions of Cu addition are the solid solution strengthening and strength enhancement of the α -Al matrix.

2.2 Grain growth in ZL201A aluminum alloy during solidification

In order to investigate the effect of Er addition on the grain growth dynamics of ZL201A alloy during solidification, the microstructures of ZL201A aluminum alloy with different Er contents were observed, as shown in Fig. 4. The microstructure of ZL201A alloy without Er addition (Fig. 4a) consists of two adjacent columnar crystal zones. The primary dendrites grow from the outer wall towards the center area, and the secondary dendrites grow perpendicularly to the direction of the primary dendrites. Once the secondary dendrites growing on adjacent pairs of primary dendrites come into contact with each other, they stop growing to form two columnar crystal zones with a distinct interface. Fig. 4b shows the microstructure of ZL201A aluminum alloy with 0.1wt% Er addition. Only a small columnar crystal region exists in the ZL201A aluminum alloy, and it is primarily distributed in the rose-shaped crystal regions, as indicated by the dashed circles in Fig. 4b. The grains are in the oval form, and the grain size is relatively large. With increasing the Er content, the number of rose-shaped crystal regions is increased, and the number of grains per unit area is also increased. It is also noted that the grain size is decreased with increasing the Er content. When the Er content reaches 0.4wt%, the grains change from coarse oval grains into fine equiaxed grains, and the microstructure is more uniform. With further increasing the Er content, the microstructure of specimen exhibits the columnar crystal region again, and the rose-shaped crystal region disappears. The grains become coarse and irregular.

Fig. 5 shows the calculation results of the average grain size

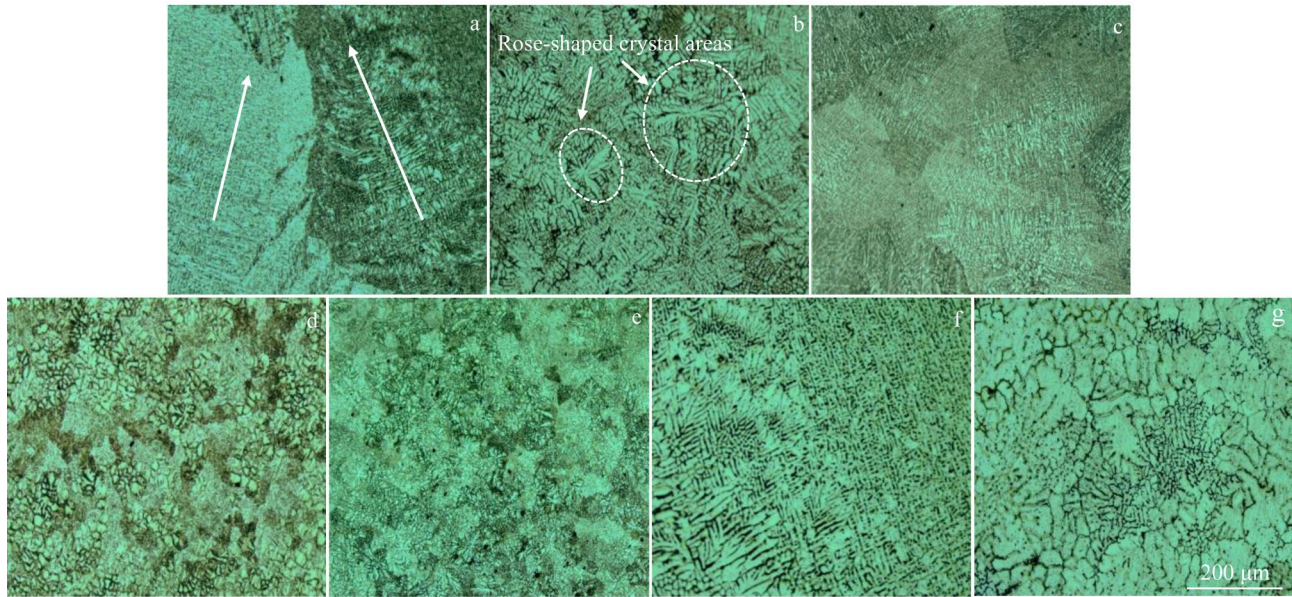


Fig.4 Microstructures of ZL201A aluminum alloy with different Er contents: (a) 0.0wt%; (b) 0.1wt%; (c) 0.2wt%; (d) 0.3wt%; (e) 0.4wt%; (f) 0.45wt%; (g) 0.5wt%

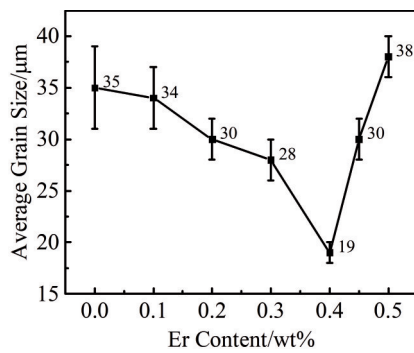


Fig.5 Effect of Er content on average grain size of ZL201A aluminum alloy

calculated with ImagePro Plus software. The average grain size of ZL201A alloy without Er addition is approximately 35 μm . With increasing the Er content from 0.0wt% to 0.4wt%, the grain size is gradually decreased. When the Er content is 0.4wt%, the average grain size is approximately 19 μm , which is smaller than that of the original ZL201A alloy by 45.71%. When the Er content exceeds 0.4wt%, the average grain size is increased.

2.3 Microstructure of ZL201A aluminum alloy

Fig. 6 shows SEM microstructures of ZL201A aluminum alloys with different Er contents. The microstructure of the as-cast ZL201A aluminum alloy consists of α -Al phase, as shown in Fig. 6a. The continuous α -Al grain boundary can be observed, and the eutectic region is composed of α -Al+ θ (Al_2Cu) and α -Al+ θ + T ($\text{Al}_{12}\text{CuMn}_2$) phases. It can be seen that a small amount of intercalated phase is formed at the grain boundary. The θ phase represents the primary strengthening phase of the ZL201A aluminum alloy, which forms a continuous mesh structure at the grain boundaries. The fine network

structure divides the matrix (Fig. 6a), reducing the strength and area of matrix phase, which is prone to dissociation fracture when the alloy is subjected to repeated impacts during service.

After Er addition, the θ phase is distributed at the points on grain boundaries rather than in the long continuous strips. However, it can be seen that the θ phase is not uniformly dispersed at the grain boundary when the Er content is lower than 0.4wt%. When the Er addition content reaches 0.4wt%, the grain size is uniform, and the θ phase is uniformly dispersed at the grain boundary. Additionally, the Er addition induces the twinning on the θ phase surface. With further increasing the Er content, a large number of bone-like regions and a small number of long features and particle-like structures appear on the grain boundaries.

Based on the abovementioned analysis and results, the Er addition induces undercooling into the alloy, resulting in the grain refinement effect on the α -Al phase. The refined grain size is related to the growth limiting factor Q , which is usually used to evaluate the growth limitation of α -Al phase grains in the alloy. Q can be calculated by Eq.(1), as follows:

$$Q = \frac{mC_0(k_0 - 1)}{k_0} \quad (1)$$

where k_0 is the solute partition coefficient, m represents the liquidus slope, and C_0 is the solute content (wt%) in the alloy. It is known that the growth limiting factor is primarily related to the solute in the alloy. At a given cooling rate, the crystal growth rate is directly proportional to the solute diffusion rate and inversely proportional to the growth limiting factor. The larger the growth limiting factor, the less the solute element diffusion, and thus the slower the crystal growth rate. This result leads to the fine grain structure. When Er content exceeds 0.4wt%, the excess Er in the

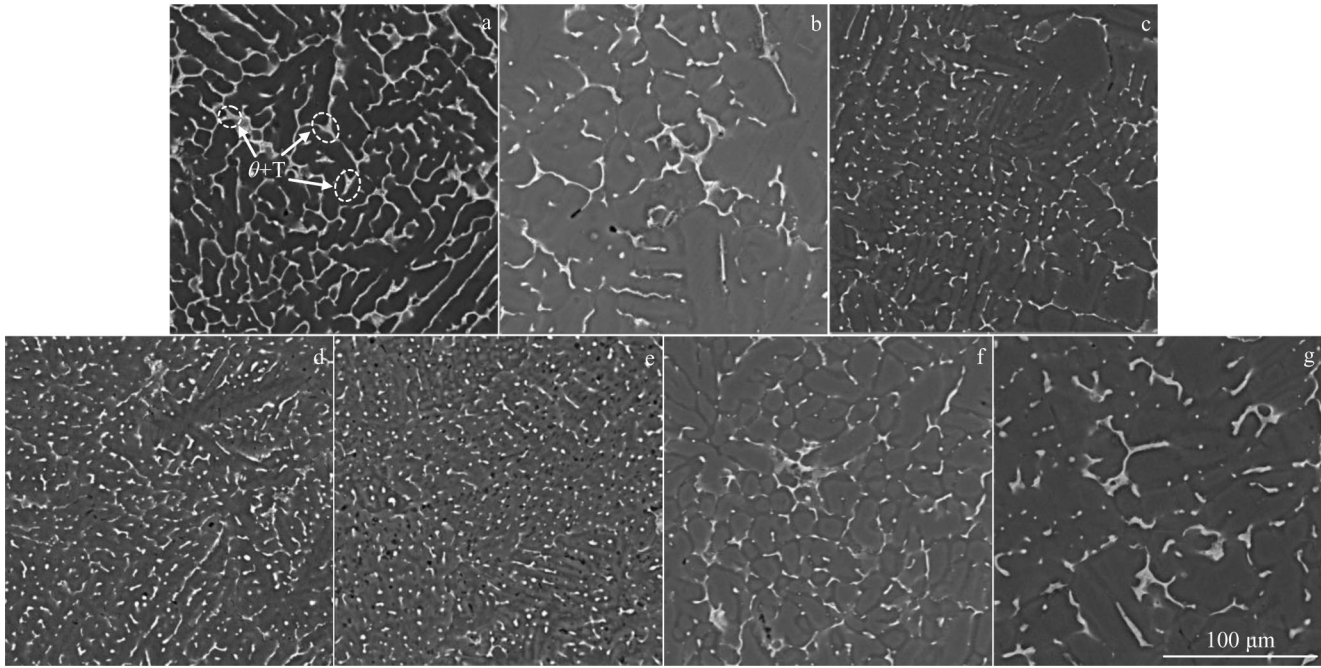


Fig.6 SEM microstructures of ZL201A aluminum alloy with different Er contents: (a) 0.0wt%; (b) 0.1wt%; (c) 0.2wt%; (d) 0.3wt%; (e) 0.4wt%; (f) 0.45wt%; (g) 0.5wt%

solidification process forms a large number of alloy compounds, and the consequent release of a large amount of latent heat of crystallization reduces the undercooling extent of liquid metal, thereby decreasing the grain refinement effect in the alloy.

Fig. 7 shows SEM microstructures of ZL201A aluminum alloy with Er content of 0.4wt% and 0.5wt%. Several points

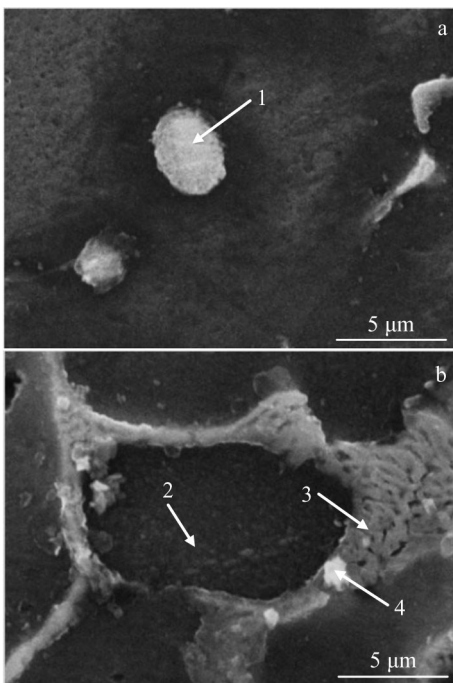


Fig.7 SEM microstructures of ZL201A aluminum alloy with 0.4wt% (a) and 0.5wt% (b) Er

were selected for EDS composition analysis, and the results of each point are shown in Table 2. It can be seen that the point 1 in Fig.7a is characterized by the white granular eutectic region with an elliptical shape and diameter of 3 μm, and it is situated at grain boundary. According to Table 2, the Er content of point 1 is only 0.1wt%. It is known that Er does not dissolve in Al at low contents, and it does not form compounds with Al. Therefore, it can be concluded that Er exists in the elemental form, providing heterogeneous nuclei for the growth of α-Al phase and increasing the number of nucleation points per unit area. According to EDS results of point 3 and point 4 in Fig.7b, Er is abundant in these regions, and the impurities, such as C, Si, O, and Fe, can also be detected. Excess Er can absorb impurity elements and form complex compounds which are distributed along grain boundaries. This formation damages the integrity of the grain boundaries, so the grain boundary strength is reduced.

The morphology of modified θ phase is changed, thereby resulting in the strengthening of alloy. Fig. 8a shows the morphology of ZL201A aluminum alloy with 0.4wt% Er addition. EDS spectrum of point 1 in Fig. 8a is shown in Fig. 8b: the Al content is 68.88wt% and the Cu content is 31.12wt% , indicating the primary strengthening θ phase (Al₂Cu) of the ZL201A aluminum alloy. The θ phase regions

Table 2 Chemical composition of point 1–4 in Fig.7 (wt%)

Point	Al	Cu	Er	Fe	C	O	Si
1	70.9	29.0	0.1	-	-	-	-
2	97.4	2.6	-	-	-	-	-
3	78.9	19.9	1.2	-	-	-	-
4	55.4	23.2	-	0.3	9.2	4.8	6.8

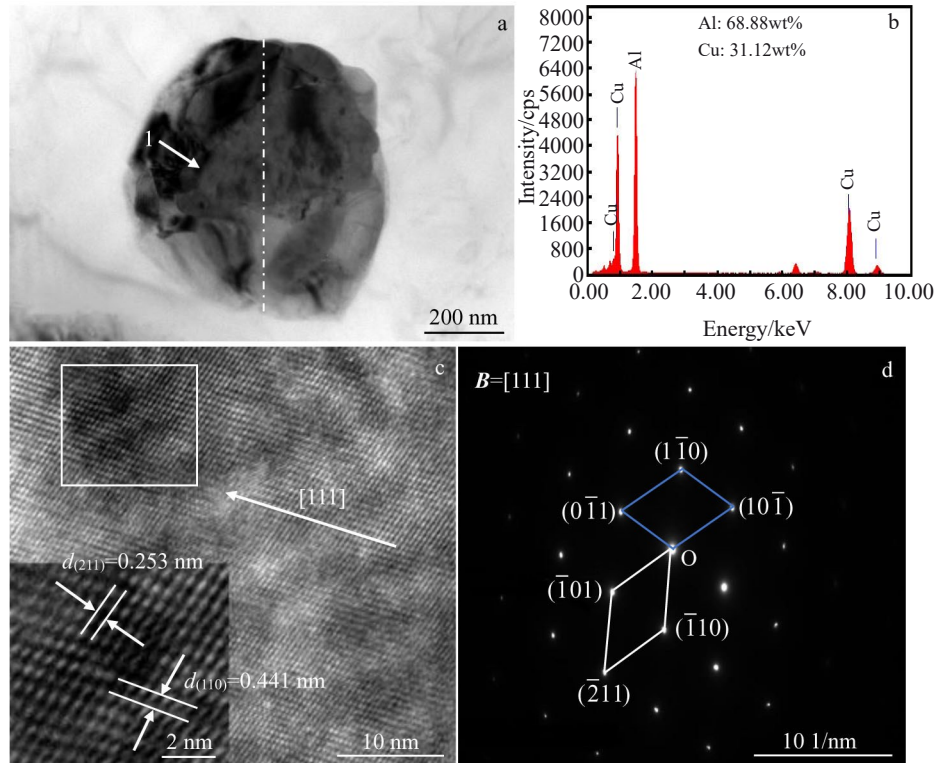


Fig.8 TEM morphology of ZL201A aluminum alloy with 0.4wt% Er (a); EDS spectrum of point 1 in Fig. 8a (b); HRTEM image and corresponding FFT pattern of θ phase (c); SAED pattern of θ phase (d)

are approximately spherical with average diameter of 697 nm. Fig.8c shows the high-resolution TEM (HRTEM) image of the θ phase. It can be seen that many high-density lattice fringes are distributed on the surface. The fringes marked by rectangle in Fig. 8c are treated by fast Fourier transform (FFT), as shown in the inset of Fig. 8c. It can be seen that two crystal planes parallel to the [111] crystal band axis can be observed, and the spacing of adjacent periodic lattice stripes is 0.235 and 0.441 nm, corresponding to the (211) and (110) crystal planes of bcc Al_2Cu , respectively. Fig. 8d shows SAED pattern of θ phase. It can be seen that $(\bar{1}10)$ and $(\bar{2}11)$ crystal planes exist in the alloy, and the diffraction spots suggest the bcc crystal with band axis of [111].

Combined with SEM microstructures of ZL201A aluminum alloy, it is found that the Er addition changes the morphology of the secondary phase from the fine network structure into fine dispersed particles. Er has high chemical activity, low potential, and particular electron layer arrangement. Therefore, Er may form stable compounds with alloy elements of high electronegativity. Generally, Er is likely to react with H_2 , N_2 , O_2 , and other gases in the melt. Such reactions may dissipate the alloy. Er not only refines the grain size of α -Al matrix, but also changes the secondary phase (θ grains) into spherical shape. With increasing the Er content, the number of α -Al grains per unit area is increased, the cracks are less, and the grain boundary strength is improved. As a result, the ZL201A aluminum alloy is strengthened by the Er addition.

2.4 Mechanical properties of ZL201A aluminum alloy

The tensile strength and hardness of the ZL201A aluminum alloy depend primarily on the size of α -Al grains, whereas the elongation mainly depends on the variation of the secondary phase morphology.

Fig. 9 shows the tensile strength and elongation of the ZL201A aluminum alloys with different Er contents. With increasing the Er content from 0.1wt% to 0.4wt%, the tensile strength and elongation of ZL201A aluminum alloy are increased. The maximum tensile strength reaches 298.14 MPa at Er content of 0.4wt%, which increases by 24.69% compared with that of the original alloy (239.11 MPa). The maximum elongation reaches 6.56%, which increases by

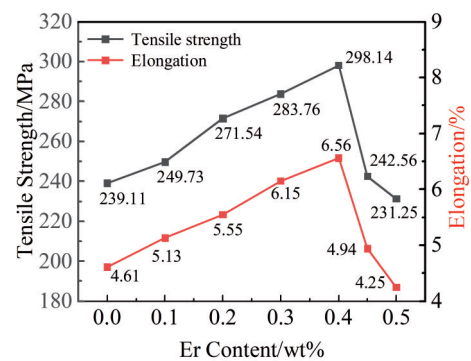


Fig.9 Tensile strength and elongation of ZL201A aluminum alloys with different Er contents

42.29%, compared with that of the original alloy. The tensile strength and elongation of the alloy are decreased with further increasing the Er content to 0.5wt% by 3.29% and 7.81%, respectively, compared with those of ZL201A aluminum alloy without Er addition.

In order to investigate the fracture mechanism of ZL201A aluminum alloy, different tensile fracture morphologies were obtained, as shown in Fig. 10. Fig. 10a shows the ZL201A aluminum alloy without Er addition. It can be seen that the fracture surface exhibits a large number of dissociation surfaces, indicating the brittle fracture. With increasing the Er addition to 0.4wt%, a large number of tough nests of small size appear and are densely distributed on the fracture surface, as shown in Fig. 10b. It is concluded that the Er addition

refines the α -Al grains, increases the elongation, and changes the fracture mode from brittle fracture to tough-brittle fracture. The fracture mode changes from tough-brittle to brittle fracture and a large number of dissociation surfaces appear when Er content exceeds 0.4wt%, as shown in Fig. 10c and 10d.

The variation in Vickers microhardness of ZL201A aluminum alloy with different Er contents is shown in Fig. 11. It can be seen that the microhardness is gradually increased from 872.2 MPa to 1107.4 MPa with increasing the Er content from 0.1wt% to 0.4wt%. The microhardness of ZL201A aluminum alloy with 0.4wt% Er is greater than that of the alloy without Er (784 MPa) by 41.25%. However, the microhardness of ZL201A aluminum alloy with 0.45wt% and

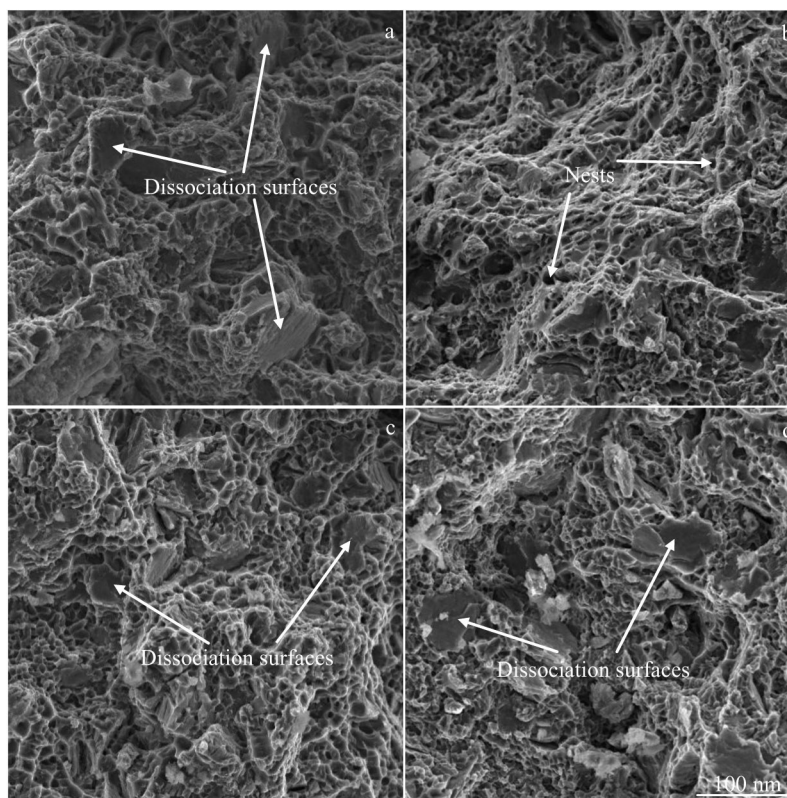


Fig.10 Tensile fracture morphologies of ZL201A aluminum alloy with different Er contents: (a) 0wt%; (b) 0.4wt%; (c) 0.45wt%; (d) 0.5wt%

0.5wt% Er decreases by 2.5% and 6.25%, respectively, compared with that of original alloy.

The grain size and mechanical properties of the alloy satisfy the Hall-Pitch relationship^[27], as follows:

$$\sigma_s = \sigma_0 + Kd^{-1/2} \quad (2)$$

where σ_s represents the yield limit of the material (MPa), σ_0 represents the intracrystalline deformation resistance, K is a constant related to the material nature and grain size, and d is the average grain diameter. It can be seen that the mechanical properties of ZL201A aluminum alloy are improved with decreasing the grain size. When Er content is less than 0.4wt%, Er exists in the elemental form in the alloy, which provides heterogeneous nucleation points for the growth of α -Al phase, therefore refining the α -Al grain and improving

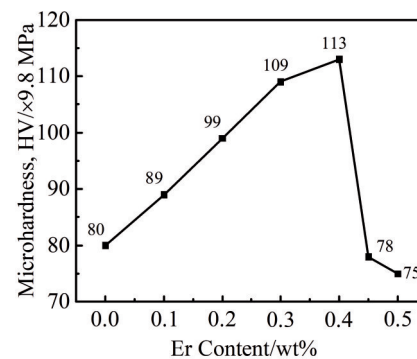


Fig.11 Effect of Er content on Vickers microhardness of ZL201A aluminum alloy

the tensile strength and microhardness of alloy. Er addition changes the θ phase grains into elliptical particles with uniform distribution at the grain boundary of matrix, which results in the dispersion strengthening and improves the elongation of the alloy. With the abovementioned mechanisms, the strength and plasticity of the alloy are improved. When the Er content is between 0.4wt% and 0.5wt%, excess Er leads to the enrichment of impurity elements, which forms complex compounds and releases a large amount of latent heat of crystallization. This phenomenon results in the reduced grain boundary strength and the undercooling of liquid metal, which weakens the grain refinement effect and decreases the strength and plasticity of the ZL201A aluminum alloy.

3 Conclusions

1) Er addition hinders the grain growth of the primary phase in ZL201A aluminum alloy and refines the grain. When Er content is 0.4wt%, the alloy microstructure is composed of equiaxed grains with uniform distribution, and the effect of grain refinement is optimal.

2) Er addition has a significant effect on the secondary phase of ZL201A aluminum alloy. The θ phase is transformed from fine network structure to small dispersed particles, and it is characterized by spherical grains. After the grain refinement, the fine and dispersed particles are uniformly distributed at the grain boundaries of matrix. Additionally, the Er addition induces the twinning to the θ phase surface.

3) With increasing the Er content, the tensile strength and elongation of ZL201A aluminum alloy are firstly increased and then decreased. The maximum tensile strength and elongation are obtained as 298.14 MPa and 6.56%, respectively, when the Er content is 0.4wt%. Compared with those of the ZL201A aluminum alloy without Er addition, the tensile strength and elongation increase by 24.69% and 42.29% after the addition of 0.4wt% Er, respectively.

4) With increasing the Er content, the Vickers microhardness of ZL201A aluminum alloy is firstly increased and then decreased. The maximum Vickers microhardness is 1107.4 MPa when Er content is 0.4wt%, which increases by 41.25%, compared with that of the original ZL201A aluminum alloy.

References

- Miller W S, Zhuang L, Bottema J et al. *Materials Science and Engineering A*[J], 2000, 280(1): 37
- Prillhofer R, Rank G, Berneder J et al. *Materials*[J], 2014, 7(7): 5047
- Zhang C, Du Y, Liu S H et al. *International Journal of Thermophysics*[J], 2015, 36(10–11): 2869
- Liu Hongliang, Shu Da, Wang Jun et al. *Materials Reports*[J], 2011, 25(5): 84 (in Chinese)
- Fu Junwei, Cui Kai, Wang Jiangchun. *The Chinese Journal of Nonferrous Metals*[J], 2021, 31(7): 1827 (in Chinese)
- Volkova E F. *Metal Science and Heat Treatment*[J], 2017, 59(3–4): 154
- She Huan, Shu Da, Chu Wei et al. *Journal of Materials Engineering*[J], 2013(6): 92 (in Chinese)
- Chang C C. *Materials Science and Technology*[J], 2013, 29(4): 504
- Kashyap K T, Chandrashekar T. *Bulletin of Materials Science*[J], 2001, 24(4): 345
- Sigworth G K. *Metallurgical Transactions A*[J], 1984, 15: 277
- Wang E Z, Gao T, Nie J F et al. *Journal of Alloys and Compounds*[J], 2014, 594: 7
- Nie Z R, Jin T N, Zou J X et al. *Transactions of Nonferrous Metals Society of China*[J], 2003, 13(3): 509
- Srikant S, Sharma V K, Kumar V et al. *Transactions of the Indian Institute of Metals*[J], 2021, 74: 2569
- Xu C, Liu Z Y, Song B et al. *Journal of Alloys and Compounds*[J], 2010, 505(1): 201
- Rshno S, Reihanian M, Ranjbar K. *Metals and Materials International*[J], 2019, 27: 1448
- Li H Y, Gao Z H, Yin Het al. *Scripta Materialia*[J], 2013, 68(1): 59
- Wen S P, Gao K Y, Li Yet al. *Scripta Materialia*[J], 2011, 65(7): 592
- Wen S P, Gao K Y, Huang H et al. *Journal of Alloys and Compounds*[J], 2013, 574: 92
- Xu Guofu, Yang Junjun, Jin Tounan et al. *The Chinese Journal of Nonferrous Metals*[J], 2006, 16(5): 768 (in Chinese)
- Xing Zebing, Nie Zuoan, Ji Xiaolan et al. *Rare Metal Materials and Engineering*[J], 2006, 35(12): 1979 (in Chinese)
- Colombo M, Buzolin R H, Gariboldi E et al. *Metallurgical and Materials Transactions A*[J], 2020, 51(2): 1000
- Booth-Morrison C, Dunand D C, Seidman D N. *Acta Materialia*[J], 2011, 59(18): 7029
- Colombo M, Albu M, Gariboldi E et al. *Materials Characterization*[J], 2020, 161: 110117
- Liang Y, Li G, Shi Z et al. *Journal of Alloys and Compounds*[J], 2022, 895(1): 162 416
- Yan J K, Chen J Y, Qiu Z S. *Rare Metal Materials and Engineering*[J], 2021, 50(12): 4314
- Wei M, Tang Y, Zhang L J et al. *Metallurgical and Materials Transactions A*[J], 2015, 46(7): 3182
- Yang H K, Cao K, Han Y et al. *Journal of Materials Science & Technology*[J], 2019, 35(1): 76

Er 含量对 ZL201A 铝合金组织和力学性能的影响

方文倩¹, 沈见冉¹, 严继康^{1,2}, 冷崇燕¹, 甘国友¹

(1. 昆明理工大学 材料科学与工程学院, 云南 昆明 650093)

(2. 西南石油大学 工程学院, 四川 南充 637001)

摘要: 通过金相显微镜、扫描电子显微镜、透射电子显微镜、能谱仪分析和力学测试, 研究了添加 Er 对 ZL201A 铝合金的微观结构和力学性能的影响。结果表明, Er 的加入使 α -Al 基体从柱状晶粒转化为细小的等轴晶粒, 同时 θ 相 (Al_2Cu) 从细小的网络结构转变为弥散细小颗粒结构。当 Er 含量达到 0.4% (质量分数) 时, 晶粒细化效应达到最大, 合金的力学性能最佳; α -Al 的平均晶粒尺寸为 19 μm ; 抗拉伸强度和伸长率分别为 298.14 MPa 和 6.56%; 断裂模式从脆性断裂转变为韧性-脆性断裂, 有利于铝合金的实际应用。当 Er 含量超过 0.4% (质量分数) 时, 合金的晶粒尺寸增大, 力学性能下降。

关键词: ZL201A; Er 元素; 晶粒细化; θ 相变质; 力学性能

作者简介: 方文倩, 女, 1997年生, 硕士生, 昆明理工大学材料科学与工程学院, 云南 昆明 650093, E-mail: 763330837@qq.com